IET Microwaves, Antennas & Propagation

Research Article

IET Journals
The Institution of Engineering and Technology

Graphene oxide-based radiofrequency identification wearable sensor for breath monitoring

ISSN 1751-8725
Received on 3rd July 2017
Revised 22nd December 2017
Accepted on 19th January 2018
doi: 10.1049/iet-map.2017.0628
www.ietdl.org

Maria Cristina Caccami[1] ✉, Mohammad Y.S. Mulla[2], Corrado Di Natale[2], Gaetano Marrocco[1]

[1]*Department of Civil Engineering and Computer Science Engineering, University of Rome Tor Vergata, via del Politecnico, 1, 00133 Rome, Italy*
[2]*Department of Electronic Engineering, University of Rome Tor Vergata, via del Politecnico, 1, 00133 Rome, Italy*
✉ *E-mail: caccami@ing.uniroma2.it*

Abstract: The monitoring of the breathing dynamic characteristics, including the presence of biomarkers in exhaled breath, is of growing interest in non-invasive diagnosis of diseases. The authors describe a wearable radiofrequency identification device hosting a flexible antenna suitable for integration into a facemask and a sensor made of graphene oxide sensitive to the humidity variations. The resulting sensor tag was characterised in reference conditions while its communication performance was estimated by electromagnetic simulations as well as measurements over a simplified model of the human head. Finally, the whole system was tested on a volunteer and was experimentally demonstrated to be capable of detecting the inhalation/exhalation cycles and abnormal patterns of respiration like the apnea by measuring the changes in graphene oxide resistance.

1 Introduction

Breath analysis is recognised as a useful indicator of a person's health status [1]. Monitoring the respiratory rate and pattern of both healthy and stressed/unhealthy individuals indeed enables an early detection of diseases and disorders, such as sleep apnea and cardiac arrest, and the characterisation of illnesses such as asthma or chronic obstructive pulmonary disease. Moreover, the identification of biomarkers and volatile organic compounds in exhaled breath is helpful in non-invasively diagnosing and monitoring of respiratory diseases such as lung cancer or ventilator-associated pneumonia. Nowadays, conventional methods of breathing monitoring involve bulky, inconvenient, and often expensive equipment that are generally incompatible with flexible wearable formats. Specifically, they require the patient to attach an uncomfortable nasal probe or cannula and to wear a chest band and sensors. Wired connections to data acquisition system and the complex circuitry prevent a long-term use required for continuous monitoring, besides creating a discomfort for the subjects [2]. Wireless and multifunctional wearable devices, capable of performing multiple actions including sensing, actuation, data storage, and energy supply, could instead be a powerful tool to enable a continuous and comfortable monitoring of breath, suitable to advance large-scale and real-time studies of the physiological processes.

This contribution addresses the wireless breath monitoring by means of radiofrequency identification (RFID) platform which, as already demonstrated in several recent papers, is becoming a valuable technology for body-centric tracking and monitoring. In particular, the paper proposes the combined use of a flexible device, operating in ultra-high frequency (UHF) RFID bands (860–960 MHz), suitable for integration into a facemask and coupled with a nanomaterial sensor made of graphene oxide (GO) [3].

Graphene is a two-dimensional (2D) nanomaterial composed of a grid of carbon atoms with sensing capabilities. The intensive research interest on the wide range of bio-applications of graphene and its derivatives is due to its outstanding physical and chemical properties and, above all, to the intrinsic biocompatibility, low-cost, and easy biological/chemical functionalisation [4]. Previous examples of sensors based on graphene functionalised with chemical/biological substances are discussed in [5, 6], respectively, for the detection of metabolites, such as the lactate, and of some pathogenic bacteria. The change in electrical conductivity of the graphene related to the variable parameter is modulated and monitored using an inductively coupled radiofrequency reader device. Among the graphene derivatives, the GO is well known to be very sensitive to water, thanks to the interactions between the exposed functional oxygen groups and water [7]. Thus, it can be considered as a promising receptor for use in wearable humidity sensors. Previous examples of GO-based sensors either involved wired connections [2, 7], or LCR meters [8] for the studies of the humidity sensing. RFID antennas fabricated using graphene flakes have been documented in the literature [9–11] with a particular focus on the impact of humidity variation effects on the antenna response. This approach has paved the way for low-cost efficient sensors suitable for healthcare applications [10] and for the Internet of Things ambient monitoring [11]. GO is, however, favourable in lieu of graphene flakes due to its stability in aqueous dispersions, thus making GO-based ink formulations suitable for large-scale printing techniques.

Nevertheless, there is still a substantial lack of a demonstration of a reliable RFID-based sensing system with GO as sensing material that is properly designed for skin adhesion. Following the embryonic experimentation in [12], this contribution hence demonstrates the first documented completely wearable, wireless GO-based breath monitoring system with UHF RFID readout in order to capture the inhalation/exhalation cycles as well as anomalous events like the apnea.

In particular, Section 2 introduces a GO-based sensor, which is sensitive to the water vapour. The sensor was manufactured and characterised in reference conditions in order to quantify how the changes in resistance of the nanomaterial are modulated by the surrounding variable relative humidity (RH). Then, a configurable radio-board antenna suitable for integrating the sensor is introduced in Section 3. Numerical results are corroborated by experimental measurements over a simplified liquid phantom. The communication performances of the wearable sensor are then discussed. Finally, the whole wireless system is tested on a volunteer and is demonstrated to be capable of detecting the dynamic characteristics of breathing (Section 4).

2 GO-based sensor

The GO sensor (Fig. 1) is composed of a Si/SiO_2 substrate with photolithographically patterned parallel Au electrodes separated by 5 μm distance. This geometry was selected after trials with interdigitated and parallel electrodes with different inter-electrode spacing. The chosen geometry provided measurable resistance of few kΩ, while other geometries resulted in very low (few 100 Ω)

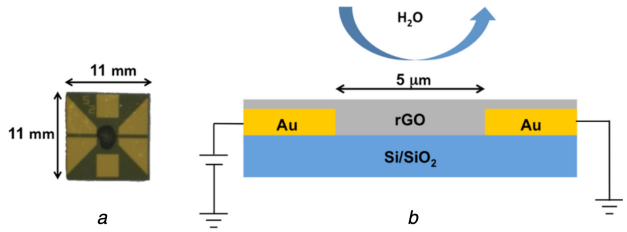

Fig. 1 *GO sensor*
(a) Prototype, ***(b)*** Its schematic cross-section including a Si/SiO_2 with p-type doped silicon wafer (300 nm SiO_2 layer) and Au 20 nm layer with 2 nm chromium adhesion promotion layer

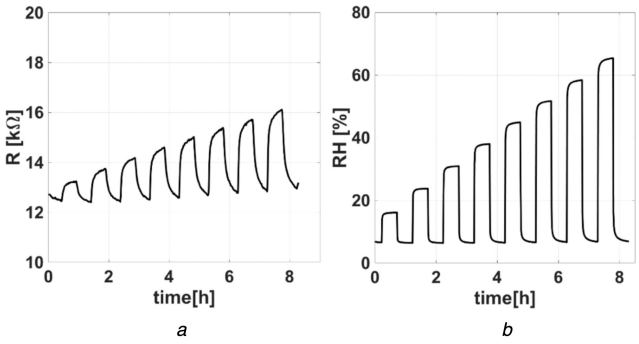

Fig. 2 *Humidity characterisation of the GO-sensor*
(a) GO resistance variation versus time when the humidity increases from the dry air value to the saturation, alternated with recoveries with dry air, ***(b)*** Humidity data versus time as detected by the E-Nose

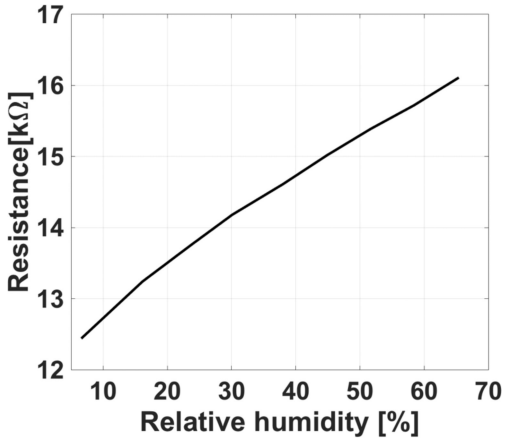

Fig. 3 *Calibration curve of R versus RH corresponding to the response shown in Fig. 2a*

or very high (MΩ) ranges. This would result in artefacts in measurement due to the influence of contact resistance effects and impedance mismatch between chip and actual sensor, respectively. A 3 µl drop of commercially available GO solution (2 mg/ml) was deposited over the electrodes by drop casting and left to dry at ambient conditions. While the GO solution was drying, 10 V peak-to-peak alternating voltage with 1 MHz frequency generated by function generator was applied between the electrodes. After complete drying, the substrate was annealed in ambient atmosphere at 195°C for 15 min on hot plate in dark.

2.1 Humidity sensing characterisation

The characterisation of the device as humidity sensor was based on the change in GO resistance due to the absorption and desorption of water vapour.

In order to test the recovery, reproducibility, and response speed to the gas under test, the sensor was exposed to cyclic increasing concentrations of humidity. In these measurements, the water molecules to be detected were separately vapourised with precisely dosed concentrations by means of a flow-system comprising a

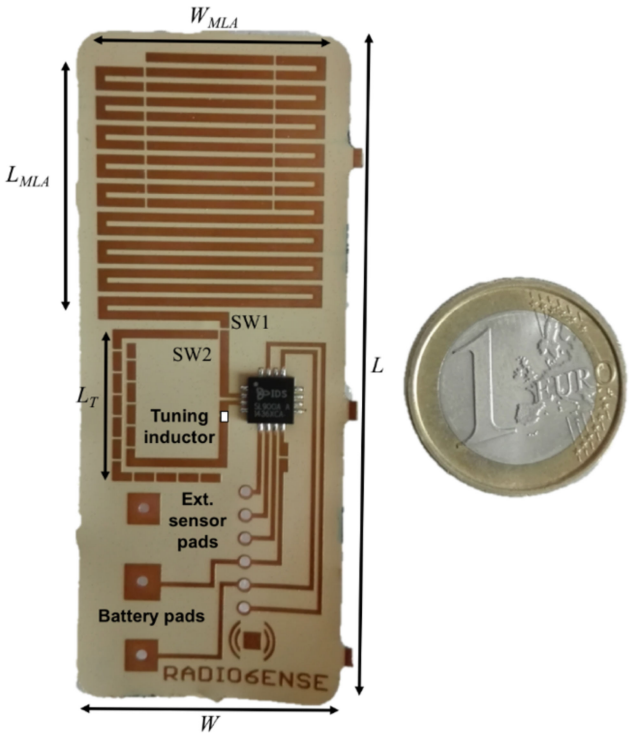

Fig. 4 *Flexible customisable antenna prototype on Kapton comprising the radiating meander line element (MLA), the spiral impedance transformer, and pads for the connections of battery and sensors. Size in mm: W = 28, L = 71, W_{MLA} = 24, L_{MLA} = 26, and L_T = 20*

mass-flow controller (MKS Instrument Inc.) and an airtight chamber, wherein the sensor was placed. The measurement protocol consisted to flow synthetic dry air through the system for 1 h to establish a system baseline, then to flow the selected dry/humid air mixture at different concentrations for 30 min (exposure time) and subsequently to flow dry air to clean the sensor surfaces for 30 min (recovery time). The profile of the resistance variation versus time with respect to the RH changes from dry to saturation is shown in Fig. 2*a*. The resistance variation follows the typical exponential profile of adsorption/desorption process. The peaks are approximately proportional to the concentration of the humidity level. The reference humidity data during the measurements (Fig. 2*b*) are provided by the *Electronic Nose* sensor [13] used as hygrometer. A drift phenomenon is visible in the graphene response thus revealing a slow recovery of the sensor to humidity. However, such a behaviour could be also correlated to other factors, for instance, the condensation effect of the water vapour deposited on the surface of the GO layer during the cycle of measurement and the presence of possible leakages through the ducts of the mass-flow controllers. Fig. 3 shows the calibration curve of the sensor, i.e. the sensor resistance versus the RH variation. The profile appears almost linear with respect to the increasing moisture levels and it is therefore possible to extract the sensitivity of the sensor, i.e. the slope of the linearised curve, as the resistance difference generated by 1% change in the RH level

$$S[R] = \frac{|\Delta R|}{|\Delta \mathrm{RH}|} = \frac{|R(\mathrm{RH_{high}}) - R(\mathrm{RH_{low}})|}{|\mathrm{RH_{high}} - \mathrm{RH_{low}}|} = 60\Omega/\mathrm{RH} \qquad (1)$$

In particular, the relative variation of the resistance is about 4 *k* Ω within humidity range from dry air to 66% RH.

3 Wearable RFID antenna

The considered RFID antenna, suitable to be worn and to host the GO sensor, is based on the configurable layout in [14] (Fig. 4) (hereafter denoted as radio-board) capable of providing the pure identification features as well as offering native integrated electronics for sensing activities.

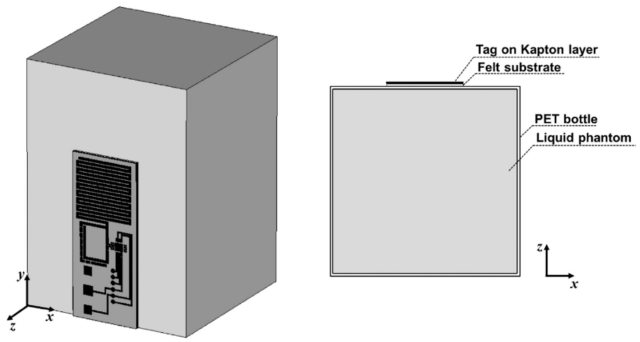

Fig. 5 *Radio-board antenna on Kapton layer attached onto homogenous liquid box resembling the human head by means of a felt substrate*

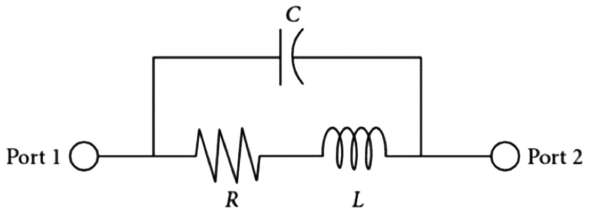

Fig. 6 *Scheme of the real inductor model*

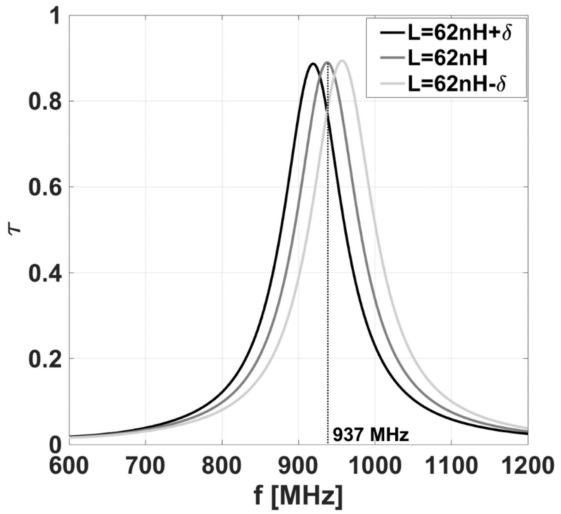

Fig. 7 *Parametric analysis of the power transfer coefficient τ versus frequency, evaluated when the tag was placed onto a homogenous liquid box, by considering a real model of the tuning inductor and a ± 5% tolerance of the declared value L = 62 nH*

The tag was manufactured by etching a flexible 50 µm-thick Kapton substrate. It comprises a radiating element made of a meander line antenna (MLA), a tunable spiral impedance transformer connected to the RFID IC and hosting an inductor for coarse tuning, and additional expansion traces for the battery and sensors interconnections. Both the MLA and the spiral traces are partly interrupted in several points with the possibility of adding lumped elements or additional metal stubs. Two further gaps (SW1 and SW2) split the transformer section from the MLA. The antenna is connected to the AMS SL900A microchip [15], which includes a 10-bit analog-to-digital converter (ADC) capable of controlling up to two analogue external sensors and even an integrated temperature sensor with programmable dynamic range between −40 and 150°C. The microchip is suitable to be used (i) in a fully passive mode (power sensitivity $P_{\text{chip}} = -6.9$ dBmW), i.e. the energy required for activation and actions is entirely scavenged from the electromagnetic waves emitted by the remote interrogator, and (ii) in battery-assisted mode ($P_{\text{chip}} = -15$ dBmW), i.e. a local battery providing additional energy for improved read range and, above all, to perform periodic measurements even in the absence of the reader (*data-logging* modality).

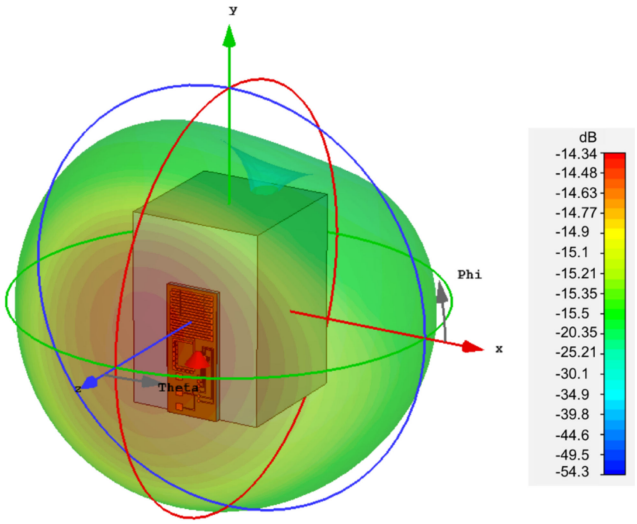

Fig. 8 *Radiation pattern of the radio-board antenna in presence of the homogenous liquid phantom simulating the human head*

3.1 Radio-board antenna configuration

The radio-board is assumed to be applied to the face by means of a facemask. Accordingly, the board resonant frequency needs to be tuned into the UHF bands for these boundary conditions. The antenna response was thus simulated by means of the finite difference time domain modelling in CST Microwave Studio 2017 implementation [16]. For the sake of the simulation speed, the tag was laid over a simplified head human phantom modelled as a hollow parallelepiped box (size: 7 cm × 7 cm × 10 cm and thickness 1 mm) made of polyethylene terephthalate (PET, $\varepsilon_{\text{R,PET}} = 2$, $\sigma_{\text{PET}} = 0.005$ S/m at 1 GHz). The parallelepiped box contained a liquid that was, in turn, modelled as homogeneous brick having average electromagnetic parameters resembling the human head ($\varepsilon_{\text{R,head}} = 41.2$, $\sigma_{\text{head}} = 0.95$ S/m in UHF RFID band) (Fig. 5). A thin felt layer ($\varepsilon_{\text{R,felt}} = 1.17$, $\sigma_{\text{felt}} = 2 \times 10^{-4}$ S/m) was used as antenna substrate with the purpose of simulating the facemask.

The performance parameter to be maximised in this configuration is the power transfer coefficient $\tau = (4R_A R_{\text{chip}} / |Z_A + Z_{\text{chip}}|^2) \leq 1$, which accounts for the impedance mismatch between the antenna and the microchip, having an RF equivalent impedance for harvesting mode $Z_{\text{chip}} = 123 - j303\ \Omega$ at 915 MHz. For this purpose, the SW1 and SW2 gaps (see Fig. 4) were configured so that the MLA section is physically connected to the input part, while the trace gaps along the MLA were left open. The antenna reactance matching was achieved by the use of a lumped tuning inductor $L = 62$ nH placed between the microchip and the antenna. The numerical simulation was led by a real inductor model (Fig. 6) with the purpose to properly account for the frequency detuning due to possible self-resonance and parasitic effects. The equivalent parasitic capacitance $C(f)$ and resistance $R(f)$

$$C(f) = \frac{1}{(2\pi f_{\text{sr}})^2 L}, \quad R(f) = \frac{2\pi f L}{Q(f)} \tag{2}$$

were hence derived by the self-resonance frequency f_{sr} and by the quality factor Q provided by the inductor manufacturer (Murata, [17]). Moreover, the above model also accounted for a maximum tolerance in the inductance value $\delta = 5\%$ with respect to the nominal value, as declared by the manufacturer. The parametric simulation of the power transfer coefficient versus frequency for such a configuration is shown in Fig. 7. The estimated resonance frequency of the tag, such that $\tau = 0.9$, is $f_0 = 937 \pm 19$ MHz, i.e. inside the North America and Japan bands.

The 3D radiation pattern of the antenna is depicted in Fig. 8, with a maximum antenna gain equal to −14.3 dB at 915 MHz, comparable with the gain of typical epidermal antennas [18].

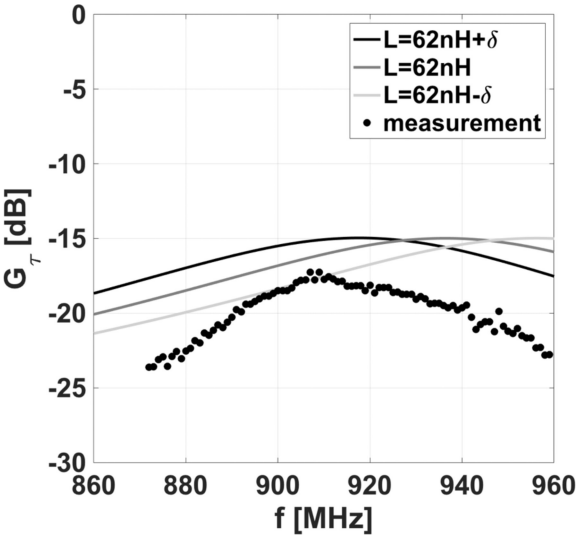

Fig. 9 *Comparison between the measured realised gain versus frequency and the corresponding simulated profiles by considering the inductance tolerance value*

Fig. 10 *Radio-board antenna and GO sensor integrated into a facemask. The measurement is performed in data-logging modality and a hand-held is used only for start/stop and data download*

3.2 Communication performance

The communication performances of the radio-board have been experimentally characterised with respect to the realised gain $G_\tau = G_{\text{tag}}\tau$, i.e. the radiation gain of the tag antenna attached over the liquid phantom reduced by the power transfer coefficient. The phantom (HSL900V2 from Speag®, [19]) consists of a water–sugar–salt mixture emulating the average dielectric properties ($\varepsilon_R = 41.2$ and $\sigma = 0.95$ S/m) of the human head within the 700–1200 MHz range. The liquid was contained within a PET bottle ($\varepsilon_{R,\text{PET}} = 2$, $\tan\delta_{\text{PET}} = 0.005$ at 1 GHz) having 1 mm thickness. The measurement setup comprised a long-range reader (*ThingMagic* Reader M5e, [20]), connected to a broadband linear-polarised stacked planar inverted-F antenna over a Forex substrate ($\varepsilon_{R,\text{forex}} = 1.55$, $\sigma_{\text{forex}} = 6 \times 10^{-4}$ S/m) with external size 13 cm × 20 cm and 5 dBi maximum gain along the broadside. The system was controlled by a custom software implementing the measurement procedure of the *turn-on* power $P_{\text{in}}^{\text{to}}$ [21, 22], i.e. the minimum power P_{in} the reader device has to emit in order to activate the tag, frequency by frequency, from a fixed reader-tag distance d. The realised gain was hence obtained from the *turn-on* power measurement by inverting the *Friis* formula

$$G_\tau = \left(\frac{4\pi d}{\lambda}\right)^2 \frac{P_{\text{chip}}}{G_R P_{\text{in}}^{to} \eta_P} \tag{3}$$

where G_R is the reader's antenna gain and η_P is the polarisation factor between the reader and the tag. The maximum value of the measured realised gain (Fig. 9) is of the order of −17.3 dB around the frequency of 915 MHz where the antenna had been specifically optimised. The measurement result was compared for corroboration with the numerical simulation accounting for the inductance tolerance $\delta = \pm 5\%$. In spite of a shift towards lower frequencies with respect to the model, the response of the radio-board prototype is comparable with the expected values. The 2–3 dB difference is probably due to a possible uncertainty on the phantom parameters that tend to degrade along with time.

By assuming 4.0 W EIRP interrogation power emitted by the reader, which is the maximum allowed according to the FCC regulations, and the chip in battery-less mode, the maximum read distance of the radio-board antenna was estimated up to 36 cm at 915 MHz (forward-link limited). Nevertheless, the maximum read range can be improved up to 90 cm, at the same frequency, by considering the use of a new family [23] of UHF microchips having an improved power sensitivity $P_{\text{chip}} = -15$ dBmW even in battery-less mode. Such a distance could be suitable for a continuous monitoring of a sleeping person by means of a reader placed close to the bed as already demonstrated for the monitoring of sleep disorders [24] and of patients' fever [25]. Nevertheless, the practical applicability of the sensor in such case must carefully account for the expected measurement and communication artefacts due to the proximity of the face with the pillow and its random motion with respect to the reader. This topic is currently outside the scope of this paper.

4 Breathing monitoring experimentation

For preliminary experiments, the GO sensor was loosely integrated to the wearable tag by connecting it to two input pins of the microchip by means of short thin wires. A custom software module enabled the settings of the corresponding sensor front-end as well as the parameters required for the acquisition data in data-logging or passive modalities. In particular, the voltage levels of the integrated ADC were individually selectable in the 50 mV steps and the current supplied to the sensor was manually selected with the purpose to define the dynamic range and the maximum resolution of the sensor [26]. The radio-board antenna was then conformed on the surface of a textile facemask, so as the GO sensor was placed in close contact with the nose, as shown in Fig. 10, in order to capture breathing sequences.

The measurements were carried out through the *data-logging* modality activated by means of a portable reader (CAEN RFID qIDmini Keyfob Bluetooth UHF RFID Reader [27]) with 1 Hz sampling rate. Accordingly, breath measurements can be comfortably performed without the need to keep the face at a given distance and orientation with respect to an interrogating fixed antenna. The tag autonomously samples the GO sensor and stores into its internal memory the digitalised resistance corresponding to the different humidity levels. The hand-held reader is instead used only to activate and terminate the measurement session and then to download the stored data from the tag's chip. At the beginning, the sensor was exposed to the ambient humidity in order to establish a baseline value. Then, we asked a volunteer to wear the facemask and to continuously and deeply breathe through the nose for a few minutes in sitting position. The subject was trained to breathe at a metronome rate according to a timed beeping sound programmed at a frequency equal to 15 respirations per minute (normal/deep breath). Fig. 11 depicts the change in GO resistance on exposure to breath. The changes in resistance for each breath cycle are clearly detectable in comparison with the signal oscillations when the sensor is at rest. The estimated maximum dynamic range of the breathing signal (82 Ω) is indeed much higher than the standard

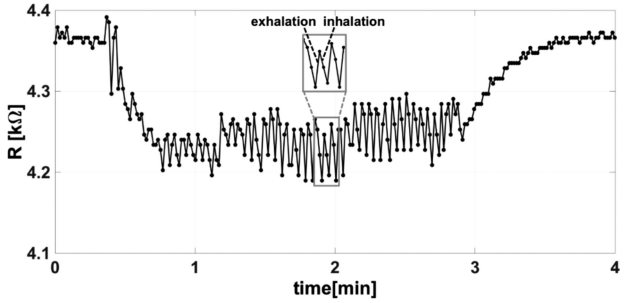

Fig. 11 *Respiratory activity of a subject recorded using a facemask with the embedded GO sensor and the radio-board antenna*

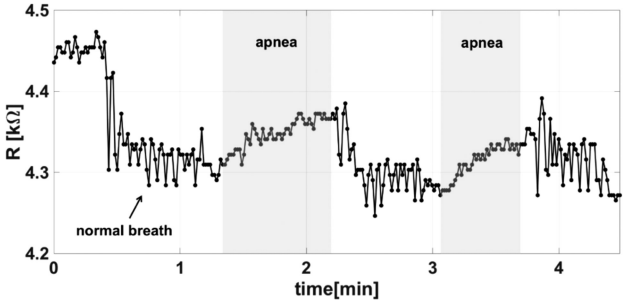

Fig. 12 *Respiratory activity by repeating apneas with short intervals*

deviation value of the noise level (4 Ω). In particular, during the breathing out, human breath is strongly humidified (RH>60%), and therefore the amount of water on the surface of the GO layer increases, and in turn its resistance. During the breathing in, the amount of water absorbed by the GO drop is instead reduced since the RH of the surrounding environment is almost always lower than the exhaled air. Fig. 11 also shows the recovery capability of the GO sensor which tends to restore back to the baseline after the breathing cycle.

Finally, we asked a subject to breathe with alternating short intervals of apneas. For simulating apnea, we requested the participant to pause their breathing for at least 60 s. The measured resistance profile, shown in Fig. 12, emphasises the capability of the sensor to detect the breathing peaks compared to the condition of apnea.

5 Discussion and conclusion

In this contribution, the advantageous sensing capabilities and the hygroscopic character of the GO were exploited in order to introduce a new class of wireless wearable RFID sensors capable of monitoring different breathing patterns. The possibility to correlate the effect of the resistance changes of the GO with the rate of respiration was demonstrated. Moreover, such a wearable RFID system may enable a simultaneous multiparameter sensing, in particular the humidity and the temperature. Additionally, since GO is rich of hydroxyl and carboxylic functional groups, further enhancement of the sensor could be achieved by covalent functionalisation of bio-receptors for the detection of cancer through breath [28]. In the next step of the research, the wireless sensor will be implemented by means of the epidermal technology so that the whole system comprising the antenna and the graphene sensor will be deposited over a thin membrane and directly stuck on the face close to the nose for a superior comfort of the user.

6 References

[1] Amann, A., Miekisch, W., Schubert, J., *et al.*: 'Analysis of exhaled breath for disease detection', *Annu. Rev. Anal. Chem.*, 2014, **7**, pp. 455–482

[2] Güder, F., Ainla, A., Redston, J., *et al.*: 'Paper-based electrical respiration sensor', *Angew. Chemie Int. Ed.*, 2016, **55**, (19), pp. 5727–5732

[3] Zhang, M., Dai, R.R., Naik, L.: '*Carbon nanomaterials for biomedical applications*', vol. 5, (Springer Series in Biomaterials Science and Engineering, Switzerland, 2016)

[4] Liu, Z.M., Shen, Z.H., Zhang, L.: 'Biomedical applications of graphene', *Theranostics*, 2012, **3**, (2), pp. 283–294

[5] Labroo, P., Cui, Y.: 'Flexible graphene bionanosensor for lactate', *Biosens. Bioelectron.*, 2013, **41**, pp. 852–856

[6] Mannoor, M.S., Tao, H., Clayton, J.D., *et al.*: 'Graphene-based wireless bacteria detection on tooth enamel', *Nat. Commun.*, 2012, **3**, (763), pp. 1–8

[7] Borini, S., White, R., Wei, D., *et al.*: 'Ultrafast graphene oxide humidity sensors', *ACS Nano*, 2013, **7**, (12), pp. 11166–11173

[8] Bi, H., Yin, K., Xie, X., *et al.*: 'Ultrahigh humidity sensitivity of graphene oxide', *Sci. Rep.*, 2013, **3**, pp. 1–8

[9] Leng, T., Huang, X., Chang, K., *et al.*: 'Graphene nanoflakes printed flexible meandered-line dipole antenna on paper substrate for low-cost RFID and sensing applications', *IEEE Antennas Wirel. Propag. Lett.*, 2016, **15**, pp. 1565–1568

[10] Akbari, M., Virkki, J., Sydänheimo, L., *et al.*: 'Toward graphene-based passive UHF RFID textile tags: A reliability study', *IEEE Trans. Device Mater. Reliab.*, 2016, **16**, (3), pp. 429–431

[11] Huang, X., Leng, T., Georgiou, T., *et al.*: 'Graphene oxide dielectric permittivity at GHz and its applications for wireless humidity sensing', arXiv preprint arXiv:1711.03435, 2017

[12] Caccami, M.C., Mulla, M.Y.S., Di Natale, C., *et al.*: 'Wireless monitoring of breath by means of a graphene oxide-based radiofrequency identification wearable sensor'. 11th European Conf. on Antennas and Propagation, Paris, France, 19–24 March 2017

[13] Gasparri, R., Santonico, M., Valentini, C., *et al.*: 'Volatile signature for the early diagnosis of lung cancer', *J. Breath Res.*, 2016, **10**, (1), pp. 1–7

[14] Occhiuzzi, C., Amendola, S., Manzari, S., *et al.*: 'Configurable radiofrequency identification sensing breadbord for industrial internet of things', *Electron. Lett.*, 2017, **53**, (3), pp. 129–130

[15] AMS SL900A Tag Chip Datasheet. Available at https://ams.com/ger/content/download/755603/1912935/file/SL900A_Datasheet_EN_v5.pdf

[16] CST Microwave Studio Suite®, 2017. Available at https://www.cst.com

[17] Murata. Available at http://www.murata.com

[18] Amendola, S., Marrocco, G.: 'Optimal performance of epidermal antennas for UHF radiofrequency identification and sensing', *IEEE Trans. Antennas Propag.*, 2017, **65**, (2), pp. 473–481

[19] Speag®, http://www.speag.com/products/dasy6/tissue-simulating-liquids

[20] ThingMagic Reader M5e. Available at http://www.thingmagic.com/embedded-rfid-readers/mercury5e

[21] Nikitin, P.V., Rao, K.V.S.: 'Theory and measurement of backscattering from RFID tags', *IEEE Antennas Propag. Mag.*, 2006, **48**, (6), pp. 212–218

[22] Marrocco, G., Amato, F.: 'Self-sensing passive RFID: from theory to tag design and experimentation'. 2009 European Microwave Conf. (EuMC), Rome, 2009, pp. 001–004

[23] Farsens RFID ICs White Paper. Available at http://www.farsens.com/en/

[24] Occhiuzzi, C., Vallese, C., Amendola, S., *et al.*: 'NIGHT-Care: A passive RFID system for remote monitoring and control of overnight living environment', *Procedia Comput. Sci.*, 2014, **32**, pp. 190–197

[25] Amendola, S., Bovesecchi, G., Palombi, A., *et al.*: 'Design, calibration and experimentation of an epidermal RFID sensor for remote temperature monitoring', *IEEE Sens. J.*, 2016, **16**, (19), pp. 7250–7257

[26] Amendola, S., Occhiuzzi, C., Manzari, S., *et al.* 'RFID-based multi-level sensing network for industrial internet of things'. in Yager, R.R., Espada, J.P. (Ed.): '*New advances in the internet of things*' (Springer, Switzerland, 2017, 1st edn.), pp. 1–24

[27] CAEN RFID R1170I - qIDmini Keyfob Bluetooth UHF RFID Reader Datasheet, Application Note. Available at www.caenrfid.it/

[28] Krilaviciute, A., Heiss, J.A., Leja, M., *et al.*: 'Detection of cancer through exhaled breath: a systematic review', *Oncotarget*, 2015, **6**, (36), pp. 38643–38657